Supporting Information

Polymer Chain Length Governs Ion Transport and Interfacial Dynamics in Aqueous Zinc-Metal Batteries

Die Luo,[a] Ben Niu,*[b] Qiurui Lin,[a] Pan Du,[a] Chen Peng,[a] and Xianru He*[a]

[a] School of New Energy and Materials, Southwest Petroleum University, Chengdu 610500, China; E-mail: xrhe@swpu.edu.cn

[b] Songshan Lake Materials Laboratory, Dongguan, Guangdong 523808, China; E-mail: niuben@sslab.org.cn

Figures

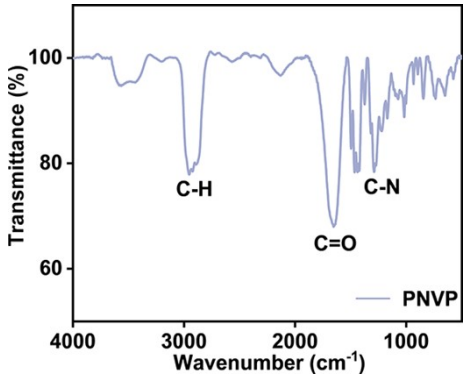

Fig.S1 FTIR spectrum of PNVP with peak assignments.

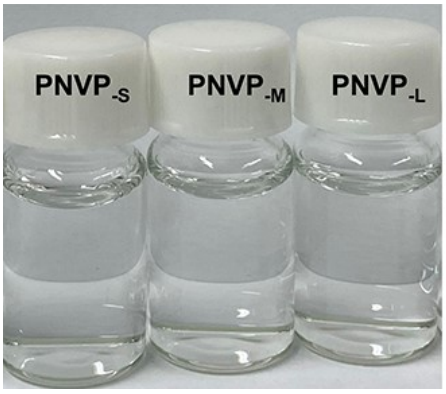

Fig.S2 Visual appearance of PNVP dissolved in pristine electrolyte.

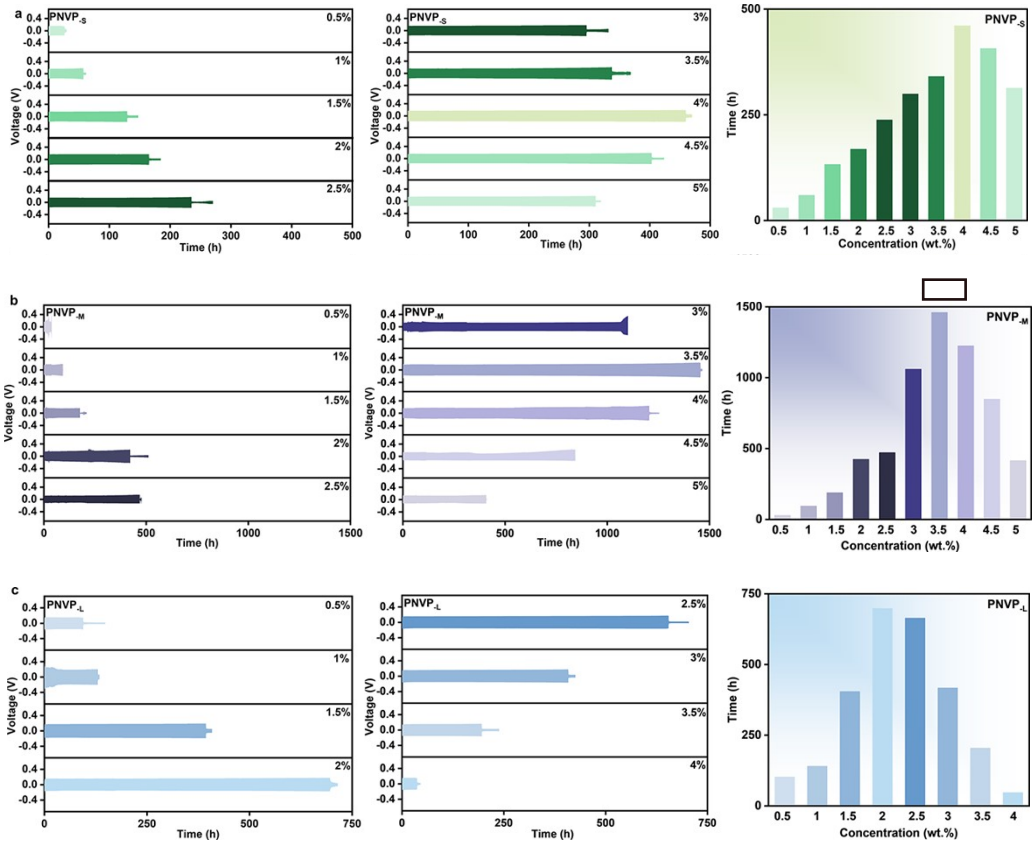

Fig.S3 Electrochemical properties of Zn-Zn symmetric cells using PNVP-containing electrolytes at a current density of 5 mA cm^{-2} with a capacity of 1 mAh cm^{-2}.

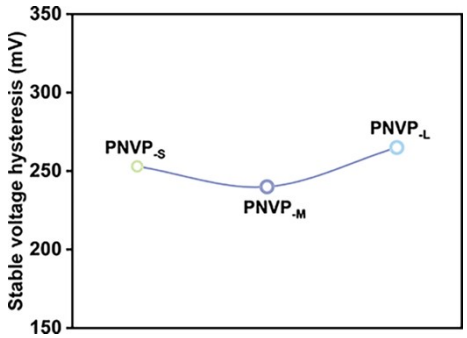

Fig.S4 Polarization voltage during stable cycling.

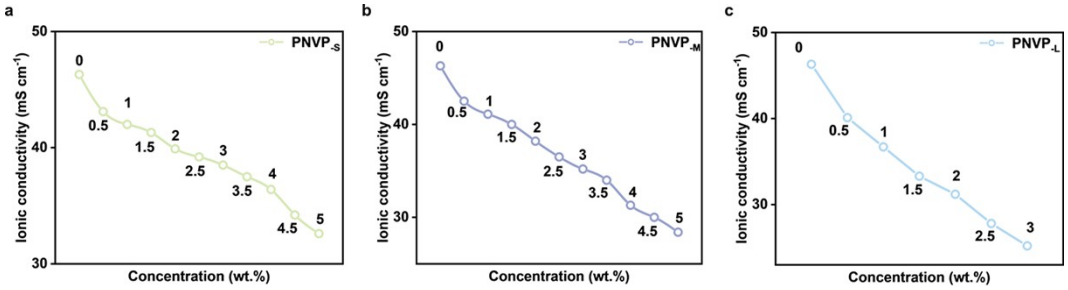

Fig.S5 Ionic conductivity of PNVP-containing electrolytes at different concentrations.

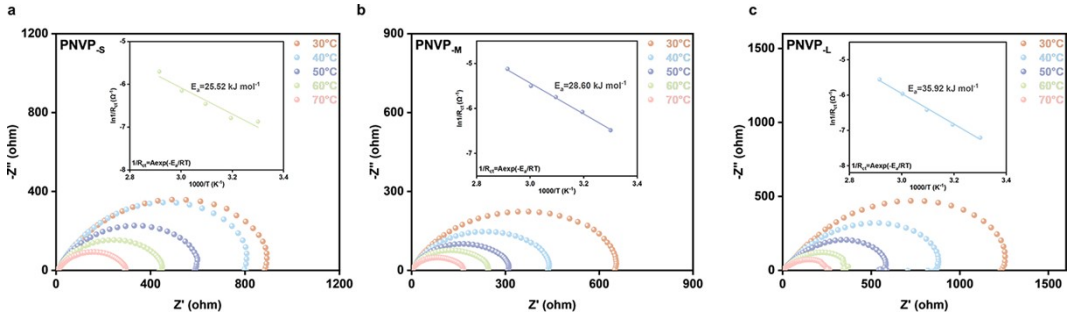

Fig.S6 Electrochemical impedance spectra (EIS) of Zn-Zn symmetric cells using PNVP-containing electrolytes, recorded between 303K and 343K to derive the Arrhenius curve and the activation energy (E_a).

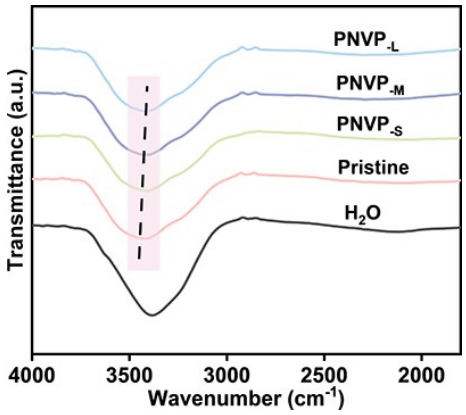

Fig.S7 FTIR spectra of the electrolytes with PNVP additive.

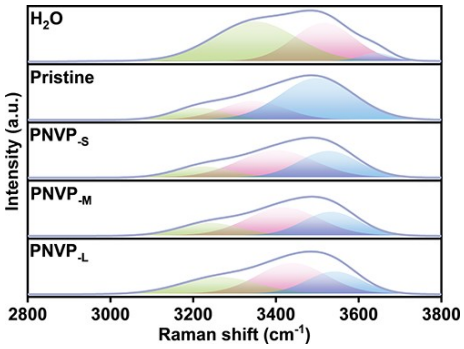

Fig.S8 Fitted Raman spectra of the electrolytes in the region of O-H stretching.

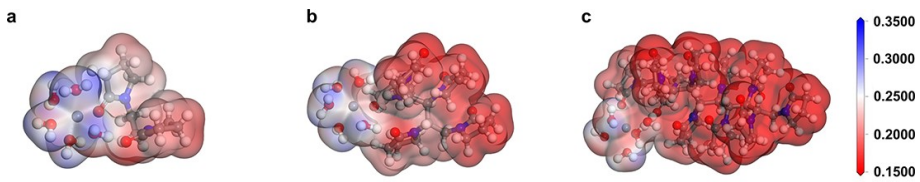

Fig.S9 Electrostatic potential maps of Zn^{2+}-$5H_2O$-$PNVP_{-S}$, Zn^{2+}-$5H_2O$-$PNVP_{-M}$ and Zn^{2+}-$5H_2O$-$PNVP_{-L}$ solvation structures.

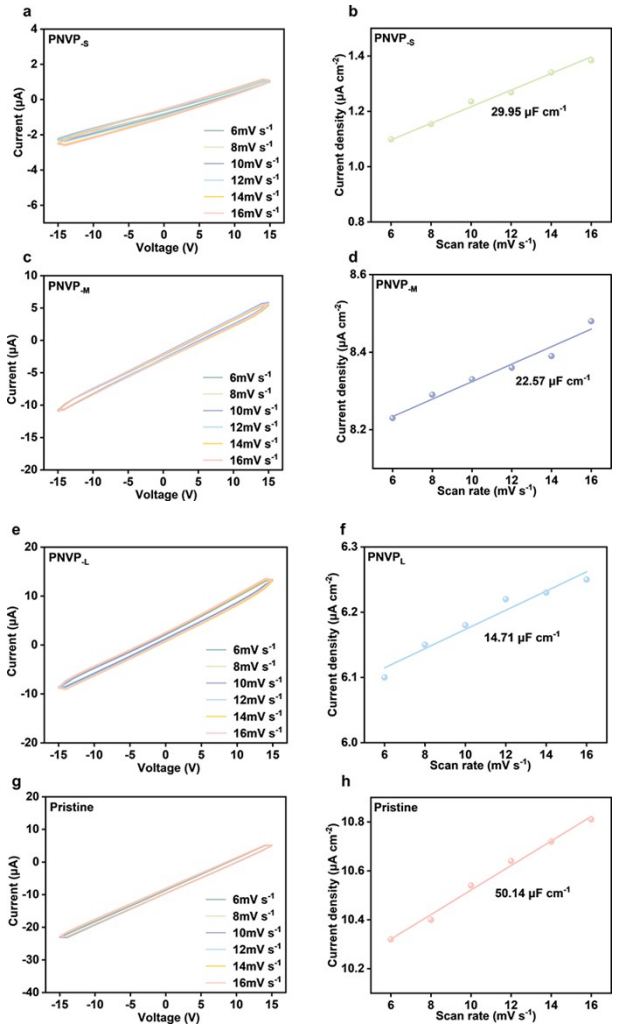

Fig.S10 Electric double layer capacitance (EDLC) measurements for Zn-Zn symmetric cells using PNVP-containing and pristine electrolytes. The EDLC is calculated through the equation C = i/v (C: capacitance, i: current. The value of i is determined by taking the half of the current difference between positive and negative scan under each scanning rate).

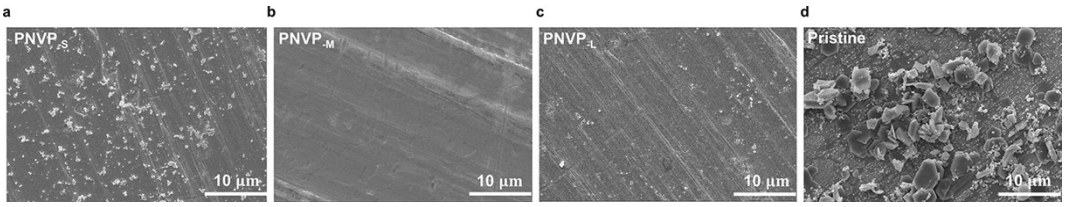

Fig.S11 SEM images of zinc-metal anodes soaked in PNVP-containing and pristine electrolytes for 7 days under 25 °C.

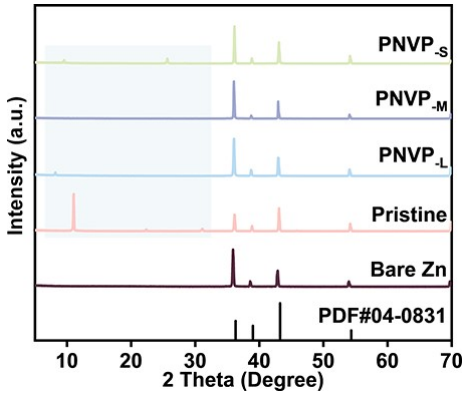

Fig.S12 The XRD patterns of zinc-metal anodes soaked in PNVP-containing and pristine electrolytes for 7 days under 25 °C.

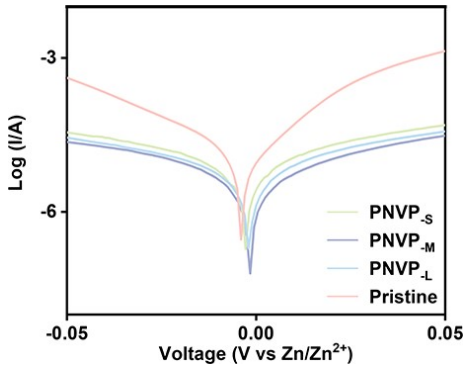

Fig.S13 Tafel plots of zinc-metal anodes tested in PNVP-containing and pristine electrolytes.

The corrosion potentials and currents of electrolytes containing PNVP with different chain lengths, as well as the pristine electrolyte, were determined by Tafel measurements. All PNVP-containing electrolytes exhibit higher corrosion potentials and lower corrosion currents compared to the pristine electrolyte. Notably, the $PNVP_{-M}$-containing electrolyte achieves the highest corrosion potential and the lowest corrosion current density. The increase in corrosion potential and decrease in corrosion current density indicate a weakening of the corrosion reaction, thereby further confirming the corrosion-preventive effect of $PNVP_{-M}$.

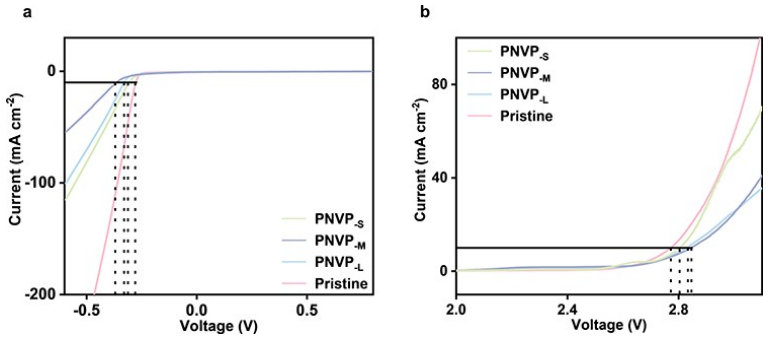

Fig.S14 (a) Hydrogen evolution reaction (HER) and (b) oxygen evolution reaction (OER) of PNVP-containing and pristine electrolytes determined using LSV at a scan rate of 1 mV s^{-1}.

As shown in Figure S14, the HER overpotential of PNVP-containing electrolytes is lower than that of the pristine electrolyte. The $PNVP_{-M}$-containing electrolyte exhibits the lowest HER overpotential. In contrast, the OER overpotential of PNVP-containing electrolytes is higher than that of the pristine electrolyte. The $PNVP_{-M}$-containing electrolyte shows the highest OER overpotential. These results indicate that $PNVP_{-M}$ is the most effective in suppressing side reactions.

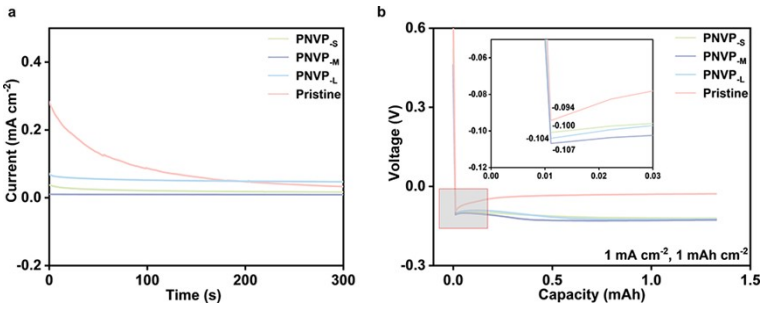

Fig.S15 (a) Chronoamperograms (CAs) under an overpotential of -150 mV. (b) Initial nucleation overpotentials of Zn plating on Cu foil in Zn-Cu asymmetric cells at 1 mA cm^{-2} with PNVP-containing and pristine electrolytes.

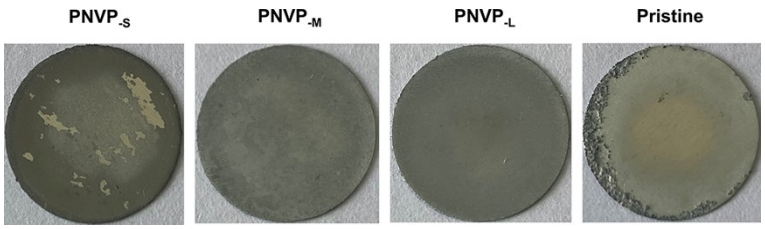

Fig.S16 Optical photographs of zinc-metal anodes in cells with PNVP-containing and pristine electrolytes after 20 cycles.

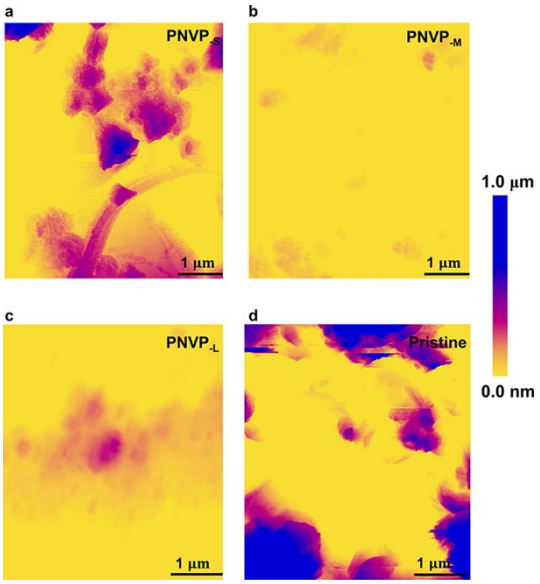

Fig.S17 AFM images of zinc-metal anodes in cells with PNVP-containing and pristine electrolytes after 20 cycles.

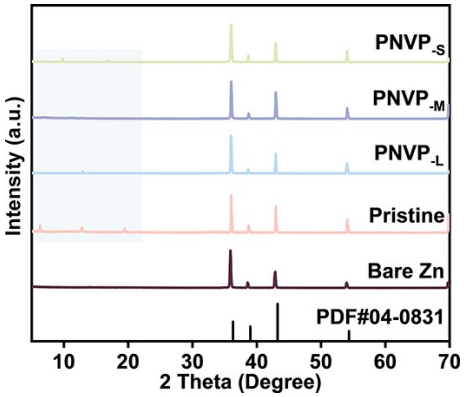

Fig.S18 The XRD pattern for the Zn deposits with 20 cycles in PNVP-containing and pristine electrolytes.

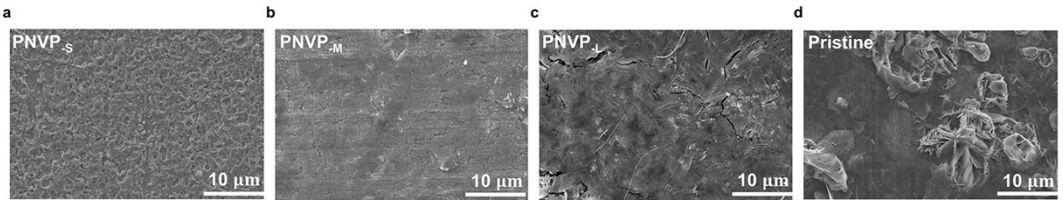

Fig.S19 SEM images of zinc-metal anodes surface from the cells cycled for 20 cycles with PNVP-containing and pristine electrolytes.

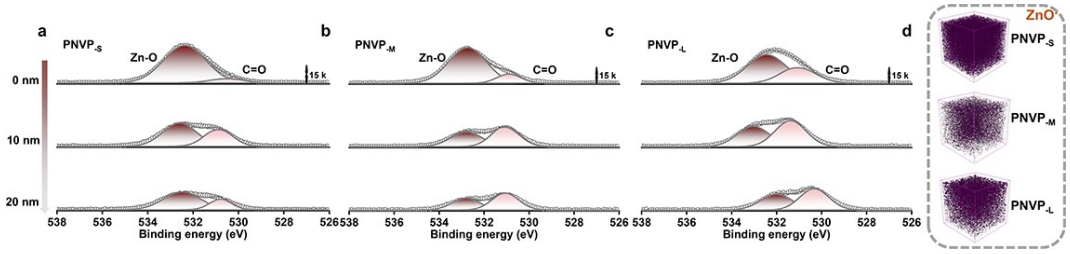

Fig.S20 (a-c) XPS depth profile for O 1s of zinc-metal anodes surface after 20 cycles in PNVP-containing at a current density of 1 mA cm^{-2} with a capacity of 1 mAh cm^{-2}. (d) Spatial distributions of zinc-metal anode surface after 20 cycles in electrolytes containing PNVP with different chain lengths (1 mA cm^{-2}/1 mAh cm^{-2}).

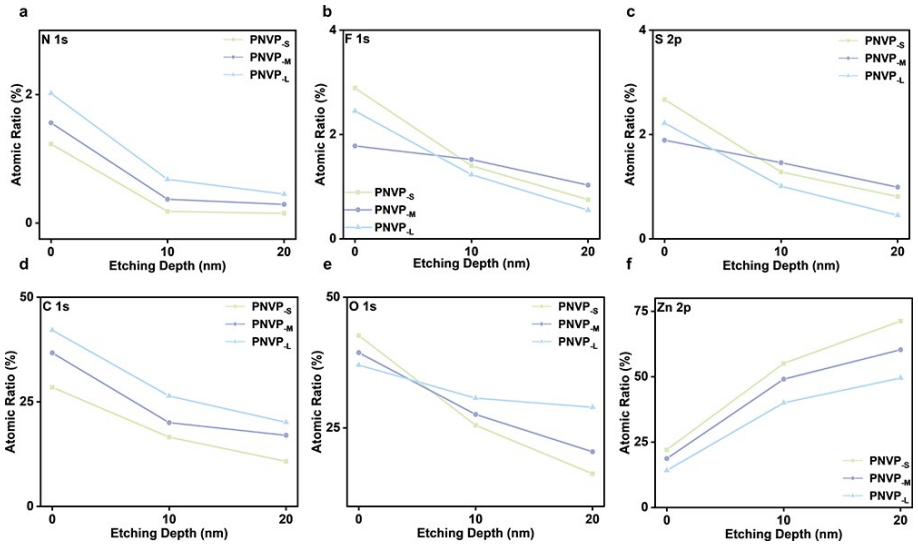

Fig.S21 Atomic composition from XPS of zinc-metal anodes surface after 20 cycles in electrolytes containing PNVP with different chain lengths.

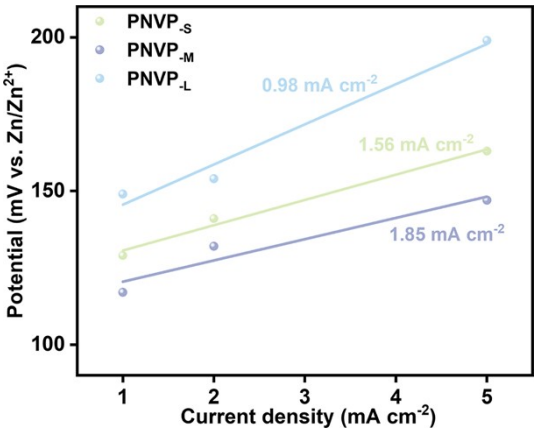

Fig.S22 The exchange current densities (i_0) of PNVP.

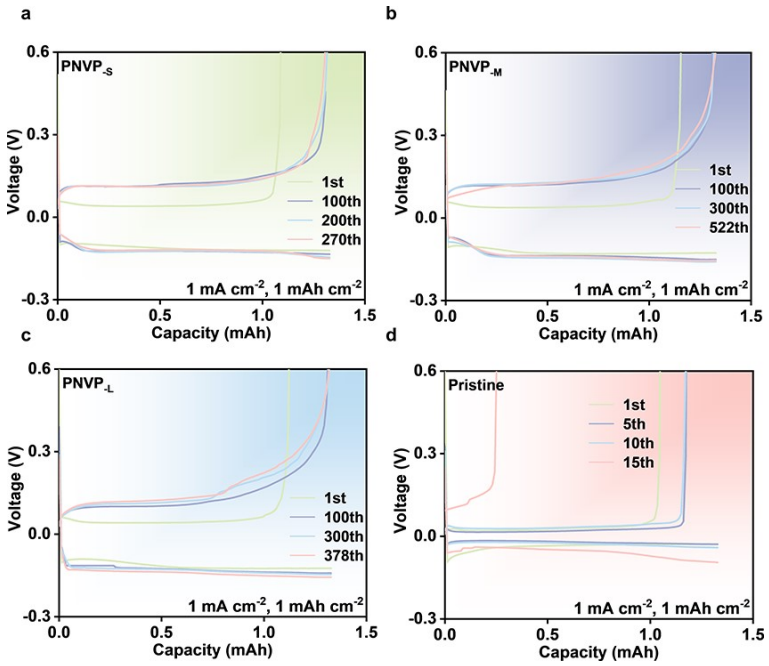

Fig.S23 Voltage profiles of Zn plating/stripping in Zn-Cu asymmetric cells at various cycles at a current density of 1 mA cm^{-2} with a capacity of 1 mAh cm^{-2}.

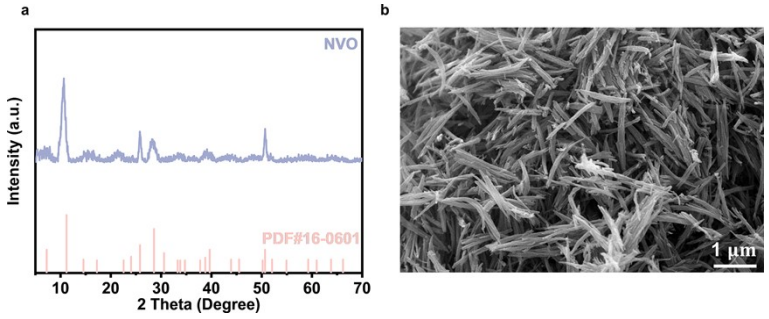

Fig.S24 (a) XRD pattern and (b) SEM image of the synthesized NVO.

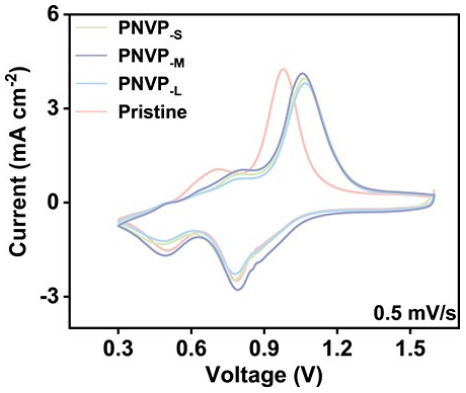

Fig.S25 CV curves of Zn-NVO batteries with PNVP-containing and pristine electrolytes.

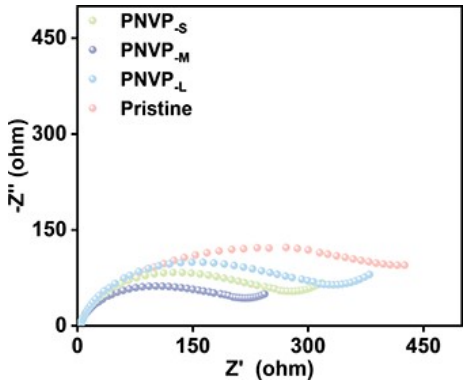

Fig.S26 The EIS curves of Zn-NVO batteries with PNVP-containing and pristine electrolytes.

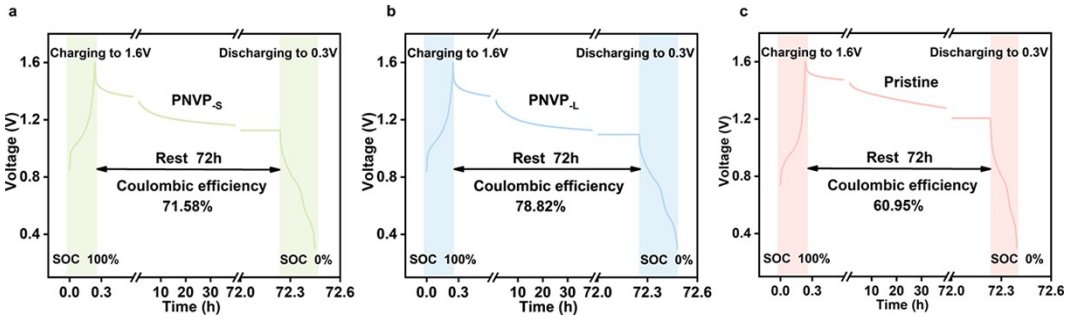

Fig.S27 Self-discharge curves of Zn-NVO batteries with PNVP-containing and pristine electrolytes.

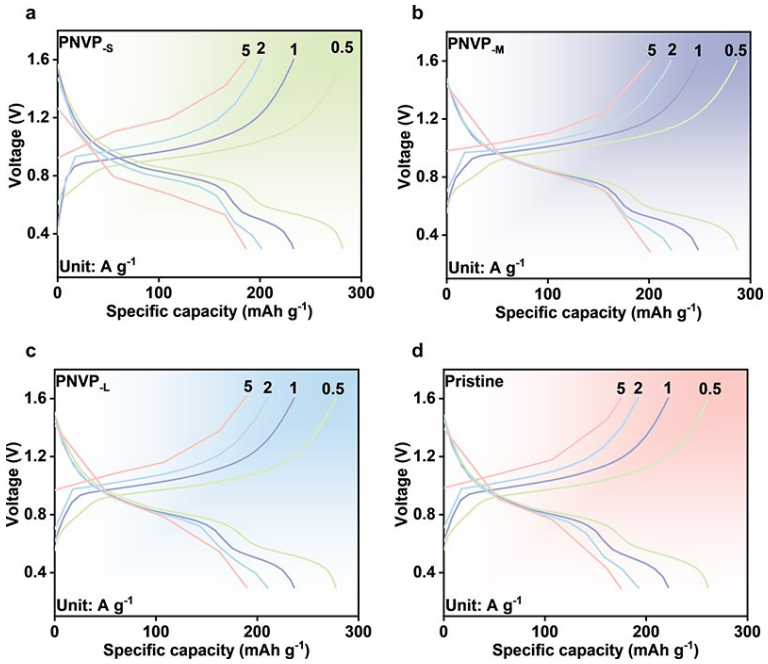

Fig.S28 Charge/discharge curves of Zn-NVO batteries with PNVP-containing and pristine electrolytes at various current densities.

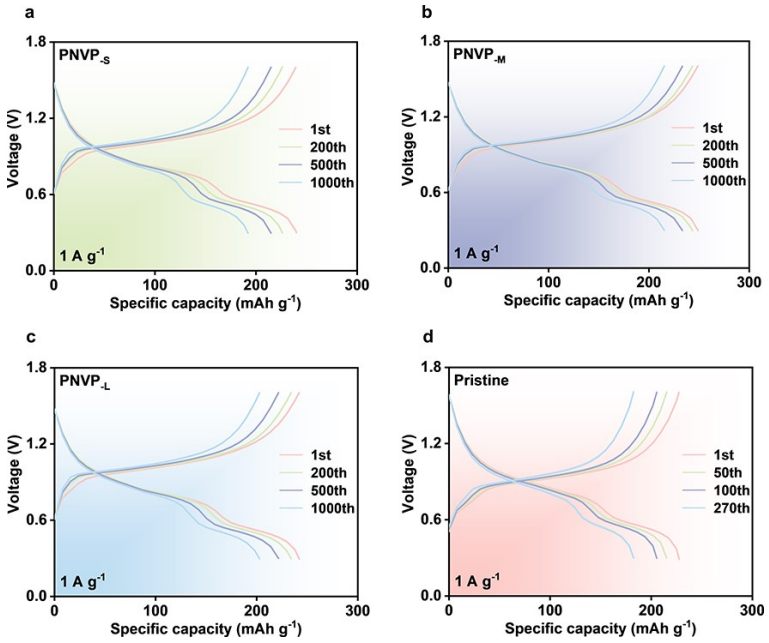

Fig.S29 Charge/discharge curves of Zn-NVO batteries with PNVP-containing and pristine electrolytes at 1 A g^{-1}.

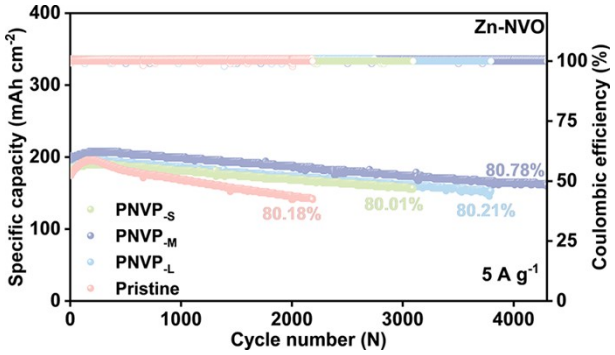

Fig.S30 Long-term cycling stability of Zn-NVO batteries with PNVP-containing and pristine electrolytes at 5 A g^{-1}.

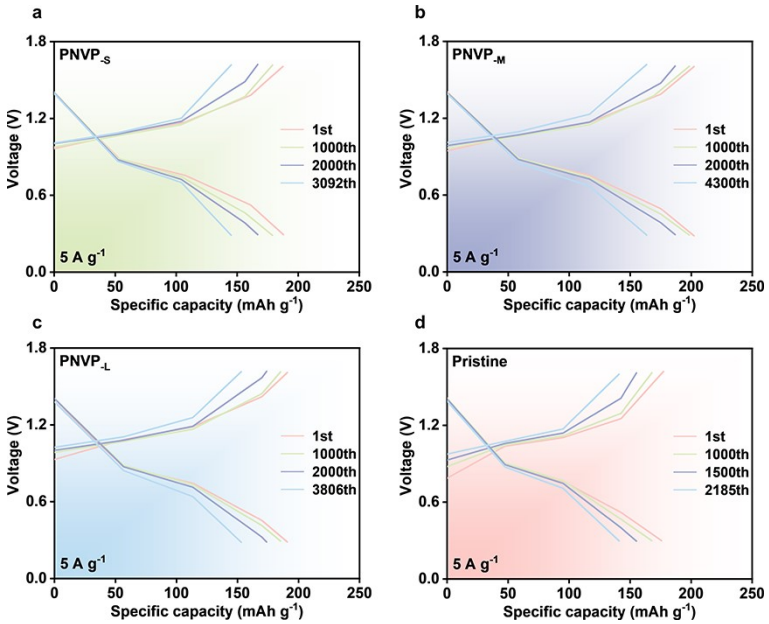

Fig.S31 Charge/discharge curves of Zn-NVO batteries with PNVP-containing and pristine electrolytes at 5 A g^{-1}.

Tables

Table S1 Molecular weight of PNVP.

Polymer	M_n (g/mol)	M_w (g/mol)	M_w/M_n	*DP*
$PNVP_{-S}$	11627	22207	1.91	105
$PNVP_{-M}$	66753	113225	1.70	601
$PNVP_{-L}$	142110	235903	1.66	1280

Table S2 Comparison cycling performance of Zn-Zn symmetric cells with different additives.

Electrolyte additive	Current density ($mA\ cm^{-2}$, $mAh\ cm^{-2}$)	Lifespan (h)	Ref.
PGA	2, 1	1600	[1]
HPMA	0.5, 0.5	3500	[2]
PVEMA	1, 1	2900	[3]
Z5S	1, 1	2768	[4]
PSS	1, 1	3000	[5]
PVA	1, 1	400	[6]
TW20	1, 1	2500	[7]
2 wt% PSS	1, 1	3000	[8]
$PNVP_{-M}$	1, 1	3600	This work

References

1 C. Huang, J. Mao, S. Li, W. Zhang, X. Wang, Z. Shen, S. Zhang, J. Guo, Y. Xu, Y. Lu, J. Lu, *Adv. Funct. Mater.*, 2024, **34**, 2315855.

2 J. Li, Y. Long, X. Yu, J. Li, N. Li, J. Han, J. Wang, Z. Yang, *Energy Storage Mater.*, 2025, **76**, 104154.

3 C. Wu, Y. Pan, Y. Jiao, P. Wu, *Angew. Chem, Int. Ed.*, 2025, **64**, e202423326.

4 F. Wu, J. Zhang, L. Ma, P. Ruan, Y. Chen, S. Meng, R. Yin, W. Shi, W. Liu, J. Zhou, X. Cao, *Angew. Chem, Int. Ed.*, 2024, **64**, e202421787.

5 Y. Wu, T. Zhang, L. Chen, Z. Zhu, L. Cheng, S. Gu, Z. Li, Z. Tong, H. Li, Y. Li, Z. Lu, W. Zhang, C. S. Lee, *Adv. Energy Mater.*, 2023, **13**, 2300719.

6 Q. Yue, Y. Wan, X. Li, Q. Zhao, T. Gao, G. Deng, B. Li, D. Xiao, *Chemical Science*, 2024, **15**, 5711-5722.

7 Q. Deng, S. You, W. Min, Y. Xu, W. Lin, J. Lu, C. Yang, *Adv. Mater.*, 2024, **36**, 2312924.

8 M. Peng, X. Tang, K. Xiao, T. Hu, K. Yuan, Y. Chen, *Angew. Chem, Int. Ed.*, 2023, **135**, e202302701.